# The Room Temperature Annealing Peak in Ionomers: Ionic Crystallites or Water Absorption?

**R. J. Goddard, B. P. Grady,† and S. L. Cooper*,‡**

*Department of Chemical Engineering, University of Wisconsin—Madison, Madison, Wisconsin 53706*

*Received July 13, 1993; Revised Manuscript Received October 7, 1993*•

ABSTRACT: A quaternized diol, 3-(trimethylammonio)-1,2-propanediol neutralized with either bromine or iodine, was used to produce a polyurethane cationomer with a poly(tetramethylene oxide) soft segment and a 4,4′-diphenylmethane diisocyanate hard segment. If these cationomers were annealed at room temperature for a period of approximately 1 month in a desiccator filled with dry $CaSO_4$, differential scanning calorimetry (DSC) studies showed an endotherm centered near 70 °C which was not present in the unannealed polymer and did not reappear upon subsequent cooling and heating cycles in the DSC. Some authors have suggested that a very similar endotherm found in other ionomers, mostly notably ethylene–methacrylic acid (E–MAA) copolymer ionomers, was due to an order–disorder transition within the ionic aggregates, i.e. ionic crystallite melting. In order to isolate the origin of this endotherm, the local environment around the anion in compression molded bromine neutralized samples was measured using the extended X-ray absorption fine-structure (EXAFS) technique. By measuring the change in the local environment over the temperature range corresponding to the DSC endotherm, it has been shown that this endotherm corresponds to water leaving the bromine coordination shell, rather than ionic crystallite melting. Other studies which include thoroughly drying the material in a vacuum oven below the transition temperature to remove the water suggest that the endotherm is due to the energetic change associated with water leaving the coordination environment of the anion in combination with water vaporization.

## Introduction

Ionomers are polymers with a small mole fraction of ionic groups covalently bonded to the polymer backbone. Because of energetic incompatibility between the polar ionic groups and the nonpolar polymer backbone, microphase separation into ionic rich domains occurs and these domains act as cross-links and reinforcing filler. This nanometer-scale morphological change leads to a dramatic improvement in material properties, including an increase in modulus, improved abrasion and tear resistance and an increase in impact strength.[1–5]

A well-known commercial ionomer is a copolymer of ethylene and methacrylic acid (E–MAA), marketed under the trade name Surlyn. Historically, E–MAA copolymers were one of the first ionomers to be studied; for example small-angle X-ray scattering investigations of E–MAA provided the first direct evidence that ionomers are microphase separated.[6] Another feature, first noticed by Marx and Cooper,[7] was an endothermic peak in differential scanning calorimetry (DSC) scans which occurred only after extended storage (1 week to 1 month) of these ionomers at room temperature. The peak was centered at approximately 50 °C and occurred over a range of approximately 20 deg. The authors attributed this endotherm to the melting of crystallites consisting of short imperfect polyethylene chains. Annealing at various temperatures above 40 °C led to a second endothermic peak located between 20 and 50 deg above the annealing temperature. This feature was assigned to lamellar thickening, and its behavior as a function of annealing temperature was shown to be qualitatively similar to the lamellar thickening endotherm normally found in intermediate and high density polyethylene.[8]

The assignment of the first peak to polyethylene crystallite melting was challenged by Tadano et al.[9,10] In plots of specific volume vs temperature, a peak was found at the temperature corresponding to the DSC endotherm, where crystallite melting would normally be seen as a discontinuity. Also, the change in the WAXS pattern after room temperature annealing was very small, certainly not large enough to correspond to the DSC endotherm. Other factors, such as an insensitivity to the position of this peak with annealing temperature, also support the conclusion that Marx and Cooper's assignment was incorrect.

Tadano and co-workers attributed this peak to an order–disorder transition within the ionic aggregates, i.e. ionic crystallite melting. Since wide-angle X-ray scattering is not sensitive to order within the aggregates (the translational symmetry within the ionic aggregates is too small to cause Bragg type reflections even if crystalline order exists on a local scale), obtaining direct evidence of ionic crystallite melting has been very difficult. Extended X-ray absorption fine-structure (EXAFS) studies were performed to determine the local order in zinc neutralized E–MAA as a function of temperature.[11] The Zn–O first-shell coordination distance ($R$) was slightly smaller at 105 °C than at room temperature. The first-shell coordination number ($N$) also increased from 4.0 to 5.0 and the Debye–Waller factor ($\sigma$) increased according to the analysis presented in that paper. However, the rise in coordination number was inconsistent with the decrease in $R$ since studies of Zn–O first coordination shells in inorganic compounds have shown that the distance increases from about 1.95–1.98 to 2.00–2.02 to 2.06–2.10 Å as zinc changes from 4-fold to 5-fold to 6-fold coordination.[12] Neutralization with a combination of zinc and 1,3-bis(aminomethyl)cyclohexane (BAC) caused a slight distortion in the zinc local environment, as evidenced by an increase in first-shell peak breadth which was attributed to an increase in the Debye–Waller factor. At 105 °C a low $R$ shoulder appeared, which the authors attributed to Zn–N first-shell coordination. The peak due to Zn–O coordination remained in the same position but the intensity of the

* To whom correspondence should be addressed.
† Present address: School of Chemical Engineering and Materials Science, University of Oklahoma, Norman, OK 73019.
‡ Present address: College of Engineering, University of Delaware, Newark, DE 19716.
• Abstract published in *Advance ACS Abstracts*, February 15, 1994.

0024-9297/94/2227-1710$04.50/0 

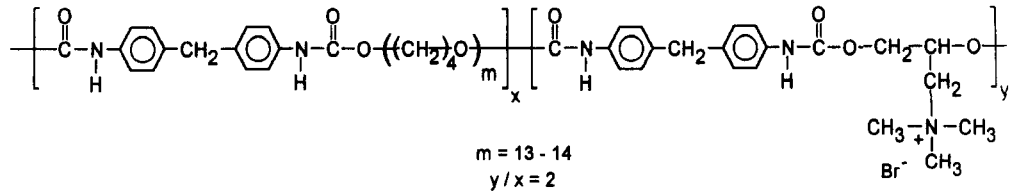


**Figure 1.** Structure of the cationomer used in this study.

peak decreased as the temperature was raised. According to the analysis, the Debye–Waller factor for the Zn–D shell increased as the temperature was raised from 25 to 105 °C while the coordination number remained constant.

Other methods have also been used to study this transition. These authors continued to investigate the effect of room temperature annealing on the mechanical properties,[10] far-infrared spectra,[13] dc conductivity,[14] dielectric relaxation properties,[15] and dynamic mechanical properties.[16] Perhaps the strongest evidence for ionic crystallite ordering was the gradual increase in modulus which occurred upon room temperature annealing. The modulus increased nearly 1 order of magnitude and the rise was correlated with the area under the DSC annealing peak. Far-infrared spectra showed a decrease in the frequency of the Zn–O vibration near 250 $cm^{-1}$ above the transition temperature. dc conductivity experiments showed an anomaly near 50 °C after room temperature annealing. Dielectric relaxation spectra do not seem to be sensitive to this transition since no clear change occurred in either $\epsilon'$ or $\epsilon''$ at the transition temperature. However, features due to polyethylene crystallite melting were very broad and may have obscured this transition. Only two-phase materials exhibited a transition in dynamic mechanical analysis (DMTA) studies while both two-phase and one-phase ionomers show the DSC annealing peak. It seems that the dynamic mechanical properties of the polymer are affected by this transition only if the material is phase separated.

The effect of room temperature annealing has been studied on E–MAA ionomers neutralized with $H^+$, $Na^+$, $K^+$, $Mg^{2+}$, $Zn^{2+}$, $Cu^{2+}$, $Mn^{2+}$, and $Co^{2+}$.[17] In all cases an endothermic peak appeared upon storage and the temperature was between 40 and 60 °C for all the neutralizing cations. If BAC was added to the polymer, the nature of the neutralizing cation affected the behavior of the modulus. In all cases the modulus initially increased with added BAC, but $Mn^{2+}$ neutralized materials exhibited a decrease in modulus above 0.5 mol of BAC/mol of carboxylate, while the modulus in materials neutralized with $Zn^{2+}$, $Cu^{2+}$, and $Co^{2+}$ either continued to increase or remained approximately constant.[18]

The addition of BAC to zinc neutralized E–MAA caused the DSC room temperature annealing peak to become larger and shifted the position to slightly higher temperature.[9] Mixing equimolar amounts of methacrylic acid and BAC in hexane followed by evaporation and subsequent storage for 7 days at room temperature resulted in an endothermic peak at 60 °C while the as-cast mixture exhibited no peak, similar to the behavior found in the ionomer.

Thirteen different amines were added to E–MAA neutralized with 0.2 mol of zinc/mol of carboxylate (the remaining groups were neutralized with $H^+$) to test the effect of amine type.[19] Compounds with two or more amine groups located on the same molecule were found to be more effective in increasing the modulus, which suggests these compounds acted as cross-linking agents. Primary or secondary amines rather than tertiary amines were also found to better promote an increase in stiffness. Finally, more rigid and higher boiling amines resulted in ionomers with a modulus higher than those of their lower boiling counterparts. However, polymeric amines decreased the modulus. For some amines, the modulus was correlated with the measured area under the annealing peak.

Up to this point, the room temperature annealing peak has been attributed to two sources, polyethylene crystallite melting and an ionic aggregate order–disorder transition. On the basis of the evidence to be presented in this publication, the room temperature annealing peak might simply be the result of water absorption from the atmosphere. This absorption occurs even when samples were stored in a desiccator with dry $CaSO_4$.

A series of papers by Painter and Coleman[20–23] found that the absorption of small amounts of water in E–MAA, which occurred when the samples were stored over anhydrous $CaSO_4$, altered the infrared absorption spectra dramatically. Upon initial cooling from the melt, relatively sharp bands were found in the region from 1500 to 1600 $cm^{-1}$ for E–MAA ionomers fully neutralized with a metal cation. After annealing for many days or weeks at room temperature, these sharp features were replaced by a broad featureless peak centered near 1550 $cm^{-1}$ (the exact position depended on the metal cation). Painter and Coleman conclusively showed that the dramatic change in the infrared spectra was due to water absorption. E–MAA ionomers neutralized with zinc did not show this effect; however the infrared spectra in this region of the original, unannealed sample was already broad and featureless. Only one set of DSC curves (for the $Ca^{2+}$ neutralized ionomer) was presented, and the same room temperature annealing peak appeared after storage for 84 days.[21] It was later shown that this sample had absorbed water, according to results from IR spectroscopy.

The effect of large amounts of water absorption on this endothermic peak has also been studied.[24] The amount of absorbed water was determined by weight loss after drying under vacuum at 450 K. The position of the room temperature annealing peak shifted from 341 K to approximately 330 K as the amount of water increased from 0.16 to 0.5 mol of $H_2O$/mol of MAA. The area under the endothermic peak also decreased rapidly over this same range. As the amount of absorbed water increased further, both the location and the area under the peak remained constant. Also in this recent paper, a revised model was presented. By analogy with sodium hexanoate, it was postulated that the endothermic peak was due to a combination of ionic crystallite melting and melting of short methylene segments which are attached to the ionic groups.

## Experimental Section

A polyurethane with a pendant quaternary amine, the structure of which is shown in Figure 1, was synthesized as a 3/2/1 copolymer of 4,4'-diphenylmethane diisocyanate (MDI), 3-(trimethylammonio)-1,2 propanediol bromide or iodide, and poly(tetramethylene oxide) (PTMO). The quaternized diol chain extender was synthesized according to the procedure originally described by Varma et al.[25] from 3-(dimethylamino)-1,2 propanediol and either bromomethane or iodomethane. Other references contain

further synthetic details[26] as well as a more complete description of the properties for this novel polyurethane cationomer.[27] DMTA measurements and DSC measurements were made on materials cast from *N,N*-dimethylacetamide (DMAC) into films approximately 0.2 mm thick. For EXAFS measurements, samples were compression molded into circular disks at 160 °C and 60 MPa for 4 min. The thickness of the disk was adjusted such that $\mu t \approx 2$ at 100 eV above the K-edge of bromine.

**Differential Scanning Calorimetry (DSC).** DSC scans were collected on a Perkin-Elmer DSC-2 equipped with a 3500 series data station. Indium was used to calibrate enthalpy measurements. Two scans from −150 to +150 °C were performed under a helium purge at a heating rate of 20 °C/min. The second scan was performed immediately after the material in the first scan was rapidly quenched to −150 °C.

**Dynamic Mechanical Thermal Analysis (DMTA).** A Rheometrics RSA II in the tension mode was used to collect DMTA spectra. The Autotension mode was used with a 120% force for pretension. Temperature steps of 3 deg with a 0.1-min soak time at a frequency of 16 Hz were used. The temperature range tested was −150 to +200 °C.

**Extended X-ray Absorption Fine Structure (EXAFS).** Most EXAFS spectra were collected at the Stanford Synchrotron Radiation Laboratory (SSRL) while a few were collected at the Cornell High Energy Synchrotron Source (CHESS). Unless otherwise noted, the data presented here were collected at SSRL. The same experimental setup was used at both facilities except where noted. The K-edge of bromine ($E_0$ = 13474 eV) was investigated. Steps of 5 eV were used in the pre-edge region and the EXAFS region, while 2-eV steps were used from −20 eV below the edge to 60 eV above the edge. Extremely narrow entrance slits (0.2 mm at SSRL, 0.5 mm at CHESS) were used in order to obtain high energy resolution. Energy calibration was performed using the sample. A 15-cm ionization chamber filled with $N_2$ and a 30-cm ionization chamber filled with Ar, both at 1 atm, were used to monitor the incoming and outgoing intensities of X-rays respectively. Spectra were collected starting at 25 °C and at 20-deg intervals thereafter until the sample began to flow on the time scale of the experiment (135 °C). Samples were heated in a specially designed cell having a temperature stability of ±2 deg. A total of 16 scans were taken at each temperature, and these scans were coadded (after $E_0$ determination) before data analysis to improve the signal to noise ratio.

## EXAFS Theory and Data Analysis

EXAFS is the measure of oscillations in the absorption coefficient ($\mu$) about its mean value at energies between 50 and 1000 eV above an atomic absorption edge. An absorption edge occurs when the energy of the X-ray is sufficient to cause the ejection of a photoelectron; the K-edge corresponds to the ejection of a 1s electron. Oscillations occur because the outgoing photoelectron wave can be back-scattered by neighboring atoms which leads to interference between the outgoing and back-scattered waves. Qualitatively, the shape and period of the oscillations will be a function of the absorbing atom as well as the type, distance and number of atoms around the absorbing atom.

The simplest correct theoretical description of this phenomena was originally developed by Stern et al.[28] and has been labeled single-electron single scattering theory. This theory assumes that multiple scattering events are unimportant and that disorders, both thermal and static, are small. The fundamental equation from this theory assuming a completely isotropic sample is

$$\chi(k) = \frac{\mu(E) - \mu_0(E)}{\mu_0(E)} = \sum_j N_j S_0^2(k) \frac{F_j(k)}{kr_j^2} e^{-2\sigma_j^2 k^2} e^{-2r_j/\lambda_j} \sin [2kr_j + \phi_{ij}(k)] \quad (1)$$

where $\mu(E)$ and $\mu_0(E)$ are the measured and mean absorption coefficients, respectively, at the energy $E$, $N_j$ is the number of atoms of type $j$ in the $j$th shell, $S_0^2(k)$ is the amplitude reduction factor which is due to excitations of electrons other than 1s electrons (for a K-edge) in the X-ray absorbing atom, $F_j(k)$ is the back-scattering amplitude from the $N_j$ atom, $r_j$ is the root mean square distance between the central atom and the $j$th atom, $\sigma_j$ is the Debye–Waller factor which measures the variation in $r_j$ about its mean, $\lambda_j$ is the electron mean free path, and $\phi_{ij}$ is the phase shift experienced by the photoelectron, which is a function of both the absorbing $i$ atom and back-scattering atom. $k$ is called the wavevector because $2\pi/k$ is the wavelength of the ejected photoelectron. Through a simple energy balance it can be shown that

$$k = \sqrt{\frac{2m_e}{h^2}(E - E_0)} \quad (2)$$

where $E_0$ is the absorption edge energy, $m_e$ is the mass of an electron, and $h$ is Planck's constant divided by $2\pi$. Generally, $F(k)$ and $\phi_{ij}(k)$ are a function of only the central and back-scattering atom and can be calculated either by theoretical means [29,30] or from model compounds. $\lambda_j$ can also be calculated either by theoretical means or from model compounds. Hence, four parameters are usually unknown for each coordination shell: $E_0$, $r_j$, $N_j$, and $\sigma_j$. Although $E_0$ can be identified from a $\mu t$ vs $E$ plot, generally $E_0$ should be allowed to vary to correct for errors in energy calibration and phase transferability.[31] The $k$ dependence of the amplitude reduction factor is usually quite small, and for the purposes of this paper, this factor will be treated as a constant. When comparing experimental data with the same absorbing atom, the amplitude reduction factor was assumed to be identical for the two samples, which is generally an excellent assumption. This factor was necessary to accurately simulate the experimental data with FEFF5. Typically, each shell is analyzed individually as will be described.

Two commercially available software packages were used for data analysis. BAN, available from Tolmar Instruments, was used for converting the measured $\mu t$ vs $E$ curve to $k^2\chi(k)$ vs $k$, subsequent Fourier transformation, isolation of each shell, back-transformation, and determination of the four unknown EXAFS parameters. This software uses the ratio method[32] to calculate $N/N_{ref}$, $E_0 - E_{0,ref}$, $\sigma^2 - \sigma_{ref}^2$, and $R - R_{ref}$ where the subscript ref represents the value for a reference compound. FEFF5,[33] available from the University of Washington, was used to theoretically calculate EXAFS spectra on the basis of the hypothesized atomic coordinates, and the values for the amplitude and phase functions were used by BAN in addition to values from model compounds.

The model compounds used in this study were tetramethylammonium bromide, sodium bromate, and carbon tetrabromide, purchased from Aldrich Chemical. The first two were dried in a vacuum oven to remove any absorbed water before use. A 90% polyethylene/10% bromine compound mixture by weight was compression molded into disks at 130 °C and 60 MPa. Preparing the model compounds in this manner allowed for easy insertion of the sample into the path of the X-ray beam.

## Results and Discussion

Quaternization of the tertiary amine group on the chain extender dramatically altered the mechanical properties of the polyurethane. At room temperature, the unquaternized material behaved as a highly viscous liquid; for example, samples stored at room temperature lost their

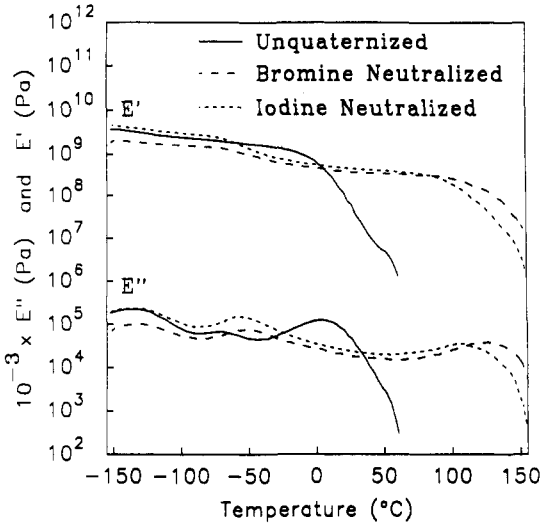


**Figure 2.** $E'$ and $E''$ for unquaternized polyurethane along with the cationomers neutralized with bromine and iodine. All samples shown in this figure were solution cast from DMAC.

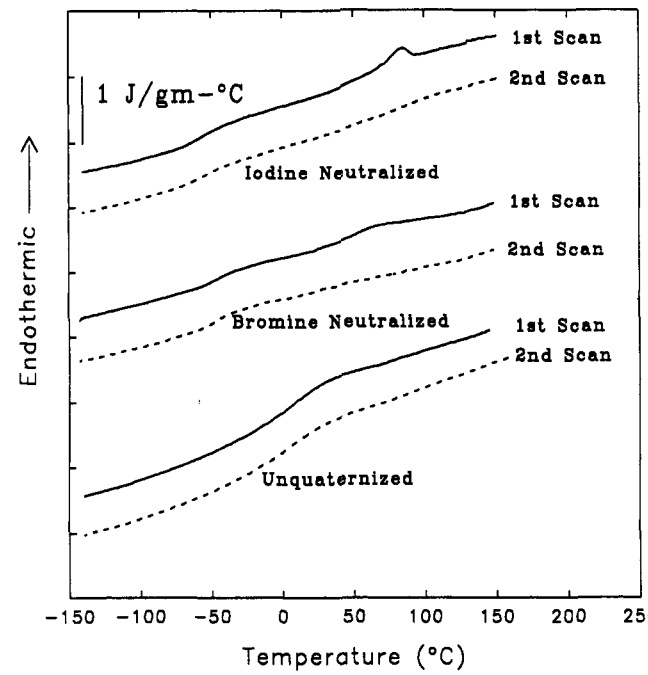


**Figure 3.** DSC results. Polymers were solution cast from DMAC, thoroughly dried in a vaccum oven to remove excess solvent, and stored in a desiccator containing dry $CaSO_4$ for 54 days.

shape over a period of a few hours. The quaternized material had the same properties as a conventional polyurethane thermoplastic elastomer, except the ionomer was slightly stiffer than typical polyurethane with the same weight percent hard segment. In the unquaternized material the pendant amino group disrupts the hard segment packing, while quaternization drives microphase separation due to the strong ionic interaction.

Figure 2 illustrates the effect of phase separation on the mechanical properties. The unquaternized material showed a small maximum in $E''$ at −70 °C, which may be due to the glass transition of a nearly pure PTMO phase. The upper transition near room temperature can be attributed to a mixed hard segment–soft segment glass transition. On the basis of these observations, the unquaternized material was primarily a mixed hard segment–soft segment one-phase material. The quaternized material showed a much larger maximum at about −45 °C followed by a transition well above 100 °C. The morphology of this material was similar to that found in conventional polyurethanes; a well phase separated material consisting of relatively pure soft segment regions and hard segment regions. On the basis of the absence of a melting transition in DSC scans, the hard segment phase was amorphous. The backbone carbon which was connected to the pendant ammonium group was asymmetric and probably not stereoregular. A full discussion of the physical properties of these materials is presented elsewhere.[27]

The room temperature annealing peak in DSC scans, with many of the same characteristics as described in the Introduction for E–MAA ionomers, also occurred in this ionomer, as illustrated in Figure 3. In the unquaternized material, the only clear transition corresponded to the mixed hard segment–soft segment glass transition discussed earlier. The heat capacity change in the unquaternized material for the PTMO glass transition was not large enough to be clearly seen in Figure 3, even though this transition was found in the DMTA spectra. Unannealed, quaternized samples only showed a soft phase glass transition near −50 °C with no other features. The absence of a hard phase glass transition in DSC spectra was not surprising since amorphous polyurethanes often show no evidence of a hard segment transition in DSC scans. After annealing for 54 days at room temperature over $CaSO_4$ in a desiccator, the initial scan showed a PTMO rich phase glass transition near −50 °C as well as an endothermic peak centered at approximately 60 °C for the $Br^-$ neutralized materials and near 80 °C for the $I^-$ neutralized materials. As indicated by Figure 2 as well as by tensile tests,[27] there was little difference in the nature or relative amount of phase separation between the bromine or iodine neutralized materials. The second DSC scan, which was collected following a rapid quench from 150 °C, showed no evidence of this endothermic peak. In order to determine the origin of this peak, EXAFS experiments on the bromine neutralized cationomer which had been stored in a desiccator over $CaSO_4$ were performed.

A short example of the analysis procedure for EXAFS data is illustrated in Figure 4 for the $Br^-$ cationomer at 25 °C. The raw $\mu t$ vs $E$ data are shown in the upper portion of Figure 4 which was then converted to $\chi(k)$ vs $k$, weighted by $k^2$, and the result is shown in the lower portion of Figure 4. $\mu_0(E)$ determination and normalization were done by fitting the $\mu(E)$ curve to a cubic spline with three sections. Because of the simple features in the XANES region, the data were truncated only 20 eV above the edge, which corresponded to $k \approx 2.3$ Å.$^{-1}$ Upper energy truncation at $k = 12.5$ Å$^{-1}$ was necessary because some data sets became noisy above this value. Fourier transformation of the $k^2\chi(k)$ vs $k$ curve resulted in the radial structure function (RSF) shown in Figure 5. The units of the abscissa of the Fourier transform are angstroms, but the peaks are shifted from the interatomic distances as indicated in eq 1: hence a subscript F will be used to distinguish this distance from the actual interatomic distance $R$. Individual peaks were isolated using a Hanning function and back-transformed for further data analysis. For the data collected at different temperatures, the regions of isolation were 0.62–1.8 Å for the first-shell peak and 2.1–2.9 Å for the second-shell peak. The identical analysis procedure was followed for all polymer samples and model compounds.

Because a visual inspection of the RSF can give qualitative information about the coordination shells around an atom, Figures 6 and 7 show the changes in the RSF as the temperature is raised to 105 °C. From Figure 3, this temperature region encompasses the DSC endothermic annealing peak. The RSF consists of two peaks, which means that there were at least two different

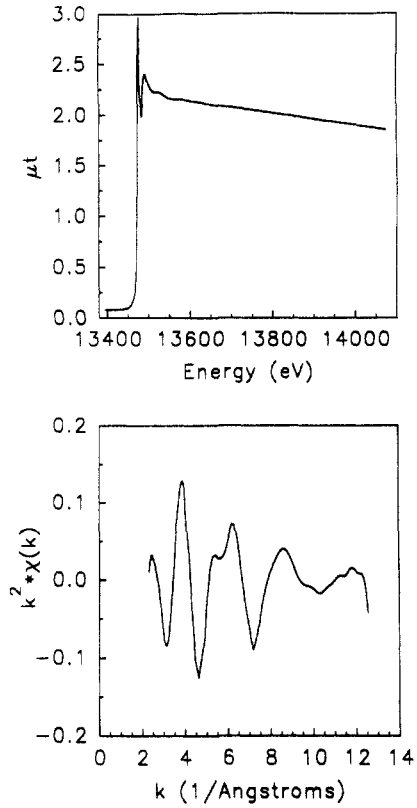


**Figure 4.** (Top) raw $\mu t$ vs $E$ and (bottom) $k^2\chi(k)$ vs $k$ for the bromine cationomer at 25 °C.

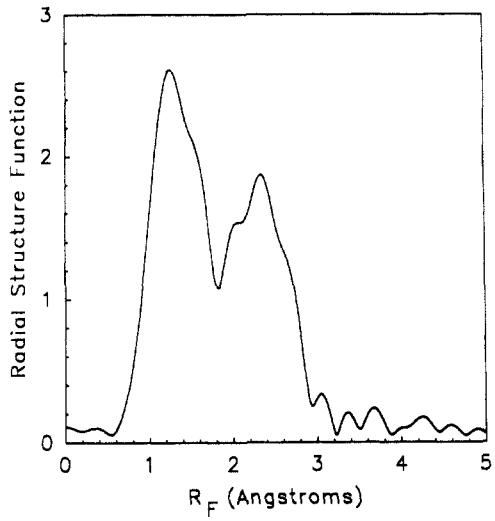


**Figure 5.** RSF for the bromine cationomer at 25 °C. This plot is the Fourier transform of the bottom plot in Figure 4.

coordination shells around the bromine. The peak at lower $R_F$ was unaffected by the change in temperature, while the second shell peak decreased in height and the position shifted slightly toward lower $R_F$ as the temperature increased. The small changes in the RSF indicate that the increase in temperature caused only small changes in the local environment. Temperature did not seem to affect the first coordination shell in any way. A shift to lower $R_F$ by the second peak suggests that the distance between the central atom and this coordination shell may have decreased, but further analysis showed that the shift in $R$ was not outside experimental error. The decrease in height indicates that the number of atoms in the coordination shell decreased and/or the Debye–Waller factor increased.

As will be discussed in detail later, each coordination shell probably was composed of more than one type of

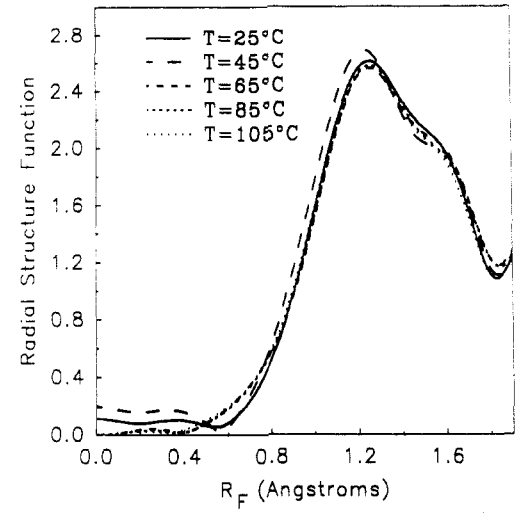


**Figure 6.** RSF of the bromine cationomer at various temperatures where both scales have been expanded to highlight the peak corresponding to the first coordination shell.

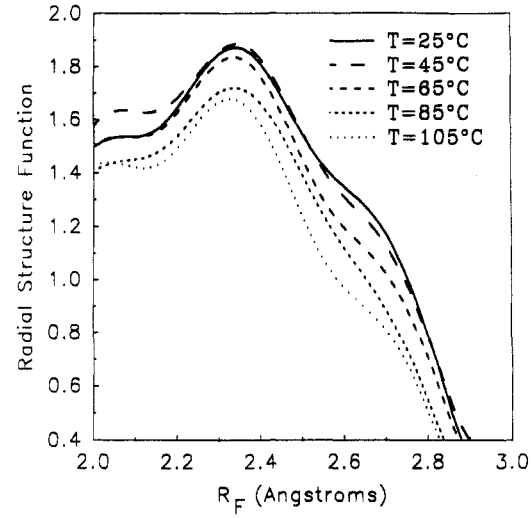


**Figure 7.** RSF of the bromine cationomer at various temperatures where both scales have been expanded to highlight the peak corresponding to the second coordination shell.

atom and/or the shell consisted of one atom but the distribution of distances was large. Either way, the ratio method cannot generally be applied to coordination shells with those characteristics. However, in this case, application of the ratio method seemed to give legitimate results, because nothing changed within experimental error except the number of atoms in the second shell. As the temperature increased, one would have expected an increase in the Debye–Waller factor. However, as was shown for lead[34] and confirmed in this study, the increase of $\sigma^2$ over a temperature range of less than 100 deg is not expected to be greater than the experimental error. $R$ also did not change significantly with temperature. Therefore, the change in the second-shell peak height was solely due to a change in coordination number. Figure 8 shows the result of the first-shell analysis; both the Debye–Waller factor and the coordination number were unchanged as the temperature increased. Error bars were calculated by assuming that all the first-shell results were identical, and these bars represent two standard deviations. The error agrees well with a much more careful calculation of the error for nickel and zinc neutralized sulfonated polystyrene ionomers.[35] The bottom curve shows a DSC scan of the compression molded material which was taken within 1 day of the EXAFS scans.

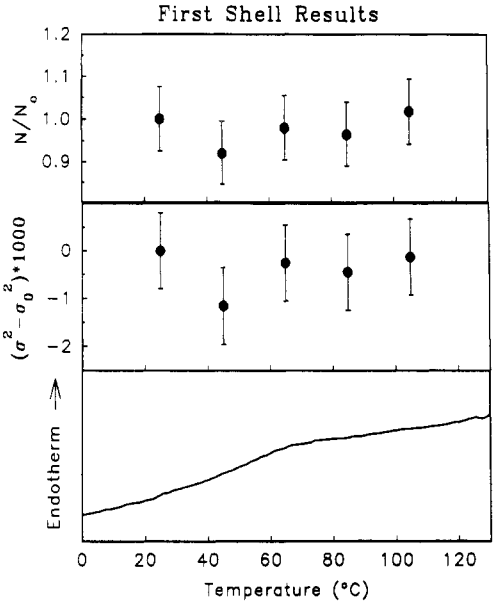


**Figure 8.** Results of the ratio method for the first shell using the data collected at 25 °C as the reference. The top plot shows the ratio in the effective coordination number while the middle plot shows the difference in the square of the Debye–Waller factor. The bottom plot shows a DSC scan of a sample which was compression molded and stored under the same conditions as the EXAFS sample. Notice the endothermic peak over the same temperature range as for the EXAFS data.

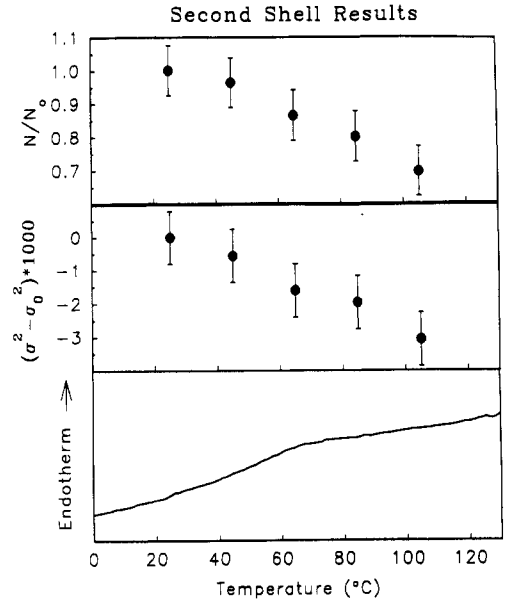


**Figure 9.** Same three plots as in Figure 8, except for the second shell.

For the second shell, Figure 9 indicates that the coordination number decreased over the same temperature range as the DSC endotherm. If the second shell was composed of more than one type of atom and only one type of atom left, the fraction of departing atoms was greater than the vertical scale indicates. By slight variation of the analysis (for example truncating at $k$ = 10 Å$^{-1}$), the vertical scale could be altered; however the effective coordination number always decreased. The behavior of the Debye–Waller factor depended on the analysis; it either remained unchanged or decreased with temperature. Finally, data from a second sample with a lower signal to noise ratio exhibited the same general trends; the first shell was unaffected while the second shell showed a decrease in peak height which the ratio method indicated was due to a decrease in coordination number.

**Table 1. EXAFS Parameters[a]**

| compd and shell | $S_0^2$ | $E_0$ (eV) | $R$ (Å) | $N$ | $\sigma^2$ (Å$^2$) |
|---|---|---|---|---|---|
| $CBr_4$[b] | 0.85 | 13480 | | | |
| C–Br | | | **1.925** | **1** | **0** |
| Br–Br | | | **3.126** | **3** | **0.008** |
| $NaBrO_3$[c] | 0.785 | 13470 | | | |
| Br–O | | | **1.65** | **1** | **0.004** |
| Br–O | | | **2.97** | **2** | |
| Br–Na | | | **3.82** | **1** | |

[a] Parameters in bold were treated as fixed since these were from crystal structures, while plain text parameters were fitted. [b] $CBr_4$ actually has four different Br–C distances and 16 different Br–Br distances which correspond to four distinct molecules within the unit cell. One of these molecules was used in the simulation. Because the arrangements are very similar, the change in the simulated pattern was small if a different molecule was used. [c] The second and third shells for $NaBrO_3$ did not have the same qualitative features as the experimental data, which can be seen by a quick inspection of Figure 11; therefore no fitting of these shells was performed.

In E–MAA, the first and only coordination shell in EXAFS studies[11] was oxygen, which did not allow unambiguous assignment of the change in coordination environment to either water evaporation or crystallite melting; however we believe that the data in that paper supports the former more than the latter. For materials with BAC, one would expect a decrease in RSF peak height if water were leaving the coordination shell in E–MAA and nitrogen were entering the coordination environment of zinc, which agrees with experimental observation. The introduction of nitrogen into the local environment of water-free zinc because of a crystallite melting process is much more difficult to rationalize, because charge neutrality must be maintained and the constancy of the radius suggests that the coordination number was unchanged. For materials without BAC, the relative insensitivity of the RSF to temperature would be expected in either case and cannot be used to distinguish between the two possibilities.

An EXAFS study of lead as the temperature was raised through the melting transition[34] indicates that the changes in the EXAFS spectra seen in this study and in the previous E–MAA study were not consistent with crystalline melting. The only consequence of melting in the EXAFS signal of lead was a discontinuous decrease in the coordination number, which the authors argued was caused by a 5 order of magnitude increase in the diffusion coefficient. Atoms which are diffusing from one site to another will not contribute to the Fourier transformed EXAFS signal, since the data do not extend to zero wavenumber. In the ionomer, one would expect little or no change in the diffusion coefficient of the atoms located in the first or second shell of the bromine upon ionic crystallite melting. One would therefore not expect any change in the first or second shells of the RSF if the endotherm were due to ionic crystallite melting, which certainly contradicts the experimental observations in both EXAFS studies.

The EXAFS patterns were analyzed more quantitatively using the simulation package FEFF5. A comparison of EXAFS patterns at the bromine K-edge of $CBr_4$ and $NaBrO_3$ to simulations showed that both positions and the number of atoms can be predicted accurately, with only the Debye–Waller factor and the amplitude reduction factor treated as fitting parameters. $E_0$ for the experimental data was determined by using the ratio method with the simulation as the reference data. The fitting results using the known crystal structures for $CBr_4$ and $NaBrO_3$ are given in Table 1, while a graphical comparison

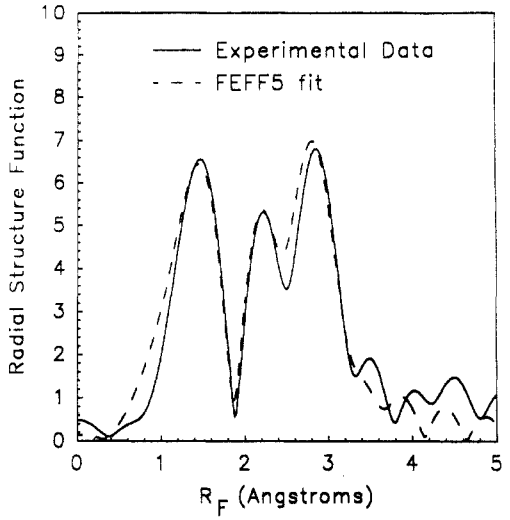


**Figure 10.** FEFF5 fit of the RSF for $CBr_4$ using the parameters listed in Table 1 compared to experimental data.

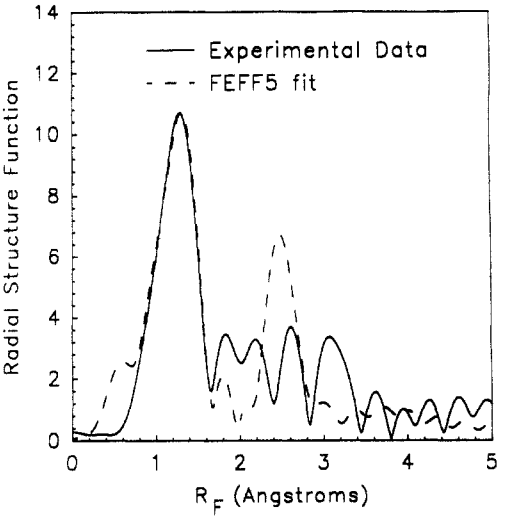


**Figure 11.** FEFF5 fit of the RSF for $NaBrO_3$ using the parameters listed in Table 1 compared to experimental data.

of the RSFs are given in Figures 10 and 11. For $CBr_4$, the agreement is excellent for all three peaks even though the crystal structure of this compound is quite complicated.[36] However, the calculated value of the Debye–Waller factor for the first shell is physically unrealistic. A slightly worse fit can be found by increasing the Debye–Waller factor for the first shell, decreasing $S_0^2$, and increasing the Debye–Waller factor for the second shell. In $NaBrO_3$, the agreement is not as good with the simulated pattern using the known crystal structure,[37] but once again the agreement for the first shell is excellent.

On the basis of the definition given earlier, the amplitude reduction factors should only depend on the central atom and hence should be identical for the two standards, which was found within experimental error. It should be emphasized that generally the fits were excellent; for example using only four adjustable parameters ($E_0$, $\sigma^2$ for the first and second shell, and $S_0^2$) the fit in Figure 10 for $CBr_4$ was produced. Also, the values for $S_0^2$ were reasonable since $S_0^2$ should fall between 0.7 and 1.0.[38] Further simulations in our laboratory of other compounds not containing bromine have shown that FEFF5 is generally quite accurate in quantitative prediction of the first two shells with reasonable fitting parameters;[35,39] in fact the disagreement in the higher shells of $NaBrO_3$ was somewhat of a surprise.

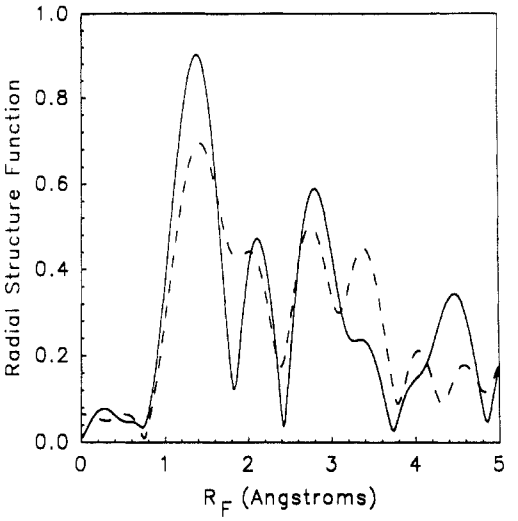


**Figure 12.** RSF for two samples of $N(CH_3)_4Br$ from data collected at CHESS. One curve is dashed while the other is solid to facilitate comparison.

The EXAFS pattern of tetramethylammonium bromide was also collected. Because of time constraints, this spectrum was collected at CHESS rather than SSRL. Unfortunately, the signal to noise ratio of this data set was much poorer than that at SSRL and the data were truncated at $k = 8$ Å$^{-1}$. The results of two different samples are shown in Figure 12. The relative error was quite large, but a quick inspection of the ordinate scale indicates that the amplitudes of the EXAFS oscillations were extremely small. The reproducibility of the position and number of peaks indicate that these features are real, but the rather large relative differences are due to the large error associated with the weak EXAFS signals.

The interpretation of the spectra of Figure 12 presents quite a problem. According to the published crystal structure,[40] the first shell for bromine should be three carbons at a distance of about 2.9 Å. According to FEFF5 simulations, the Br–C distance indicated by Figure 12 is approximately 1.95 Å, which is identical to the ionic radius of $Br^-$ and is very close to the bond distance in $CBr_4$. On the basis of the good agreement with the other two standards, it is extremely unlikely that FEFF5 is in error. X-ray scattering is only sensitive to Br atoms, since the scattering power of bromine is much higher than that of carbon or nitrogen. Therefore the Br–C crystallographic distance in ref 40 was inferred from the unit cell of the atoms coupled with the position of the bromine atoms. Raman spectra of these materials have shown that the $N(CH_3)_4$ tetrahedral is greatly distorted after the introduction of $Br^-$ atoms,[41] which supports the hypothesis that the simple interpretation of the X-ray scattering spectra may have been incorrect with regard to the Br–C distance. These EXAFS results suggest that the C–Br distance may be much closer than previously thought and the bond between bromine and the tetramethylammonium ion must be at least partially covalent, which is not inconceivable on the basis of the Raman results. The second-shell distance of 2.8 Å seems reasonable for Br–N, if the first-shell distance is 1.95 Å.

However, $S_0^2$, which is approximately 0.07, is much too small to suggest that this simple interpretation is correct. Because $S_0^2$ was reasonable for the standards, it is again extremely unlikely that the software is wrong. Another explanation would be that a small percentage (about 10%) of the atoms are in this covalent bonded structure while the remainder of the atoms are in the published crystal structure. This interpretation cannot fully describe the

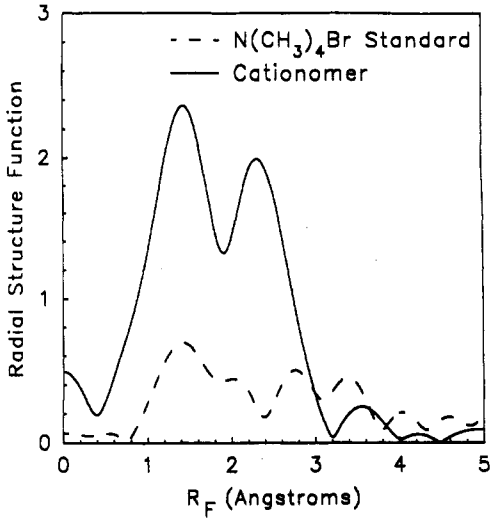


**Figure 13.** Comparison of the RSFs for $N(CH_3)_4Br$ and the cationomer in Figure 5. The latter curve and the curve in Figure 5 are not identical because the raw data were truncated at $k$ = 8 Å$^{-1}$ for the RSF shown in this figure.

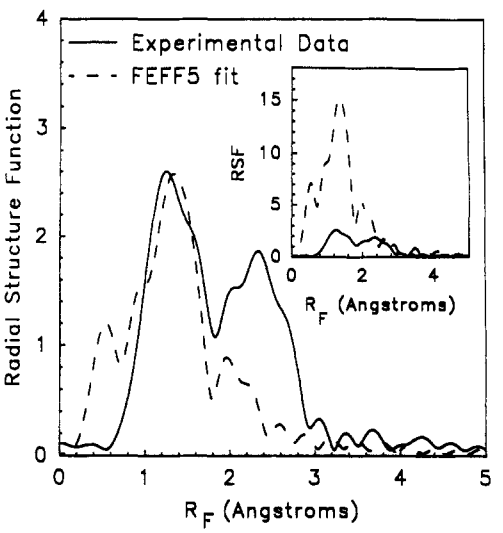


**Figure 14.** FEFF5 fit for the RSF shown in Figure 5 with a Debye–Waller factor of 0.005 for both shells and $S_0^2$ of 0.13. Other parameters are discussed in the text. The inset shows the fit if $S_0^2$ is set equal to 1, which clearly illustrates the problem with RSF peak heights and FEFF5 simulations discussed in the text.

experimental results either since a Br–C distance of 2.9 Å with 90% of the molecules in this configuration would produce a large peak near the observed second-shell peak, and hence, $S_0^2$ still would have to be extremely small. As shown by Stern et al.,[34] an atom which spends much of its time diffusing from one site to another will not exhibit EXAFS oscillations since the analysis does not include data near zero wavenumber. However, in a solid material, this explanation makes little sense. At this time, we are unable to explain the reason for the extremely small amplitude reduction factor. The important conclusions for this paper are that the peaks in the standard are real, the peaks in the standard and the cationomer are close to the same position, and the peak heights for both the standard and the ionomer are much smaller than predicted.

The data used to create Figure 5 were truncated at $k$ = 8 Å$^{-1}$, and a RSF was created to compare the standard to the cationomer, a comparison shown in Figure 13. The first-shell peaks are in the same position in both spectra but the second-shell peak is shifted. As discussed previously, the quality of the data for the standard is lower and this undoubtedly accounts for some of the shift. The presence of water in the ionomer may also shift the second peak position, as will be discussed below. The difference in peak heights between the cationomer and the standard cannot be explained at this time. The local environment in the cationomer seems similar to the standard, but there are substantial differences, as indicated by the stronger oscillations in the cationomer.

The first shell in the cationomer is probably composed of carbon. On the basis of stoichiometry and tetrahedral symmetry, one would expect three carbon atoms per bromine atom. Simulations indicate that if the first shell is composed of carbon, there are 0.5 carbon atoms for every bromine atom. Therefore, a Br–C first shell is inconsistent with respect to FEFF5 simulations; however the choice of any other atom in the first shell also suffers from this disagreement in peak heights. In addition, the width of the first-shell peak, particularly the marked asymmetry toward higher $R_F$, indicates at least two different Br–C distances. On the basis of the peak and shoulder positions, the range in the Br–C distance seems to be 1.92–2.05 Å. Figure 14 shows a simulation of three carbon atoms at 2.02 Å, with a second shell consisting of one Br–N atom at a distance of 2.33 Å, which is the absolute minimum distance for Br–N based on space filling calculations given published C–N bond distances and the distance to the first shell.

In the second shell, simulations indicate that a Br–C, Br–N, or Br–O RSF peak will be centered at nearly the same $R_F$ if the atomic distances are identical. Since these atomic combinations are the only logical possibilities, the middle of the broad second shell corresponds to a distance of approximately 2.8 Å. The width of the second-shell peak suggests that the second shell is composed of one atom at more than one distance or two different atoms. At this point, our postulate is that the second shell is due to at least two different types of atoms, one of which is oxygen from water. A Br–O distance of 2.8 Å is reasonable given the respective radii of bromine and water.

Even though our understanding of the underlying structure is incomplete, these findings conclusively show that the room temperature annealing peak in these cationomers is a result of water absorption rather than crystallite formation. To further establish this fact, a sample was allowed to anneal in a desiccator for approximately 9 months. Then the sample was dried for 1 week in a vacuum oven held at room temperature, which is below the transition temperature. The melting phenomenon is essentially independent of pressure over this pressure range; hence if the transition were due to crystallite melting one would have expected no change in either the EXAFS spectra or the DSC spectra after this treatment. In order to facilitate mass transfer of water, the sample was in the form of flakes rather than compression molded disks. EXAFS patterns collected at CHESS of the dried vs undried material as shown in Figure 15, agree qualitatively with the data collected at SSRL as a function of temperature; namely, the second-shell peak decreases in height upon drying or upon heating while the first-shell peak changes very little. Peak position shifts may not have been observed for the SSRL samples because the initial water content as well as the amount of evaporated water was much greater for the vacuum treated samples, as indicated by the ratio of the first- to second-shell peak height. The shift in position of the second-shell peak in Figure 15 also corroborates the hypothesis that the second shell in Figure 5 is due to at least two atoms. Perhaps even more convincing that the endothermic peak was due to water comes from the result that no DSC endothermic peak was found in the vacuum-dried material. Finally,

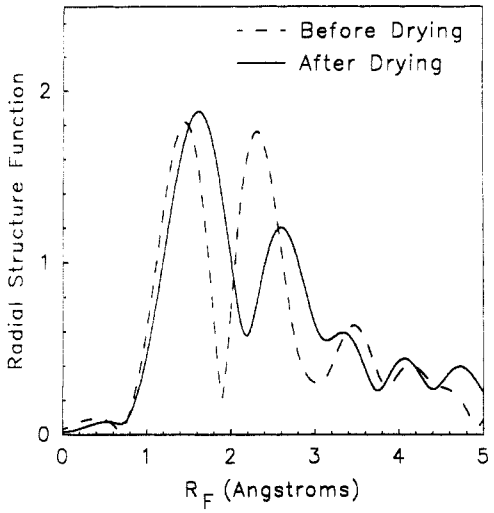


**Figure 15.** RSF of the cationomer before and after drying for 1 week in a vacuum oven at room temperature from data collected at CHESS.

the weight loss after drying was found to be 0.84% which corresponds to 0.5 $H_2O$ molecules for every bromine atom. The RSF peak height from FEFF5 simulations for a Br–O coordination shell located at 2.8 Å with 0.5 oxygens for every bromine was consistent with Figures 5 and 15 using reasonable values for the Debye–Waller factor and $S_0^2$. This agreement was in stark contrast to the 0.5–1 order of magnitude difference in the peak heights for any reasonable Br–C or Br–N combination in the first and second shells for both the standard and the cationomer.

In light of our conclusions for the polyurethane cationomers, other data presented in ref 9–19 and 24 were reexamined. Certain observations in those papers seem consistent with water desorption rather than ionic crystallite melting as the cause of the room temperature annealing peak in E–MAA ionomers.

More specifically, (1) when E–MAA was annealed at room temperature, the DMTA $E''$ feature due to this transition appeared, yet did not appear after annealing at −5 °C.[16] Since there is no evidence to support any thermodynamic change in the material between these two temperatures, it is difficult to rationalize this result in terms of crystallite melting. However, if water absorption was causing the feature, then the low absolute humidity of air at −5 °C would have meant that little water could be absorbed by the polymer.

(2) The temperature of the transition in E–MAA was almost independent of the type of metal cation, and the temperature was far below that of the small-molecule analogue. If the transition were due to ionic crystallite melting, then one would expect some dependence on metal cation type, since the melting point of similar small-molecule compounds certainly depends on the metal cation. For example, the oxides of sodium, copper, zinc, and magnesium melt at 1275, 1326, 1975, and 2850 °C respectively, while the carbonates of lithium, sodium, and potassium melt at 723, 851, and 891 °C, respectively. If the transition were a result of water absorption or crystallization of methylene segments, as proposed in the revised model,[24] then the temperature should be nearly independent of the metal cation type and would fall in the 50–80 °C range.

(3) The addition of BAC increased the endothermic peak height.[9] Because of the amine functionalities, the BAC selectively partitions to the ionic aggregates. One has a very difficult time understanding how a bulky organic molecule increases the crystallinity within an aggregate, which must occur if the endothermic transition is attributed to ionic crystallite melting. In terms of water absorption, the amine functionality provides two more energetically favored sites for water. Also, BAC presumably decreases the packing density within the aggregates, which reduces steric restrictions, hence allowing more water inside the aggregate. Finally, if some of the BAC is in the polymer matrix, then this molecule should plasticize the ethylene phase, which should increase the diffusion constant of water through the organic phase. All of these factors would tend to support a hypothesis of water absorption rather than ionic crystallite melting as the cause of the annealing endotherm in E–MAA ionomers.

As properly noted by one reviewer, not all the results in these previous references support water absorption. Perhaps the strongest evidence against this interpretation for E–MAA ionomers was the dramatic change which occurred after cold drawing.[17] Both the position and the area under the endothermic peak decreased substantially after cold drawing, neither of which is consistent with water absorption. Also, the recent introduction of a model which includes contributions from methylene sequences[24] raises possibilities not addressed by this current work. With a more complex morphology which includes matrix crystallization, perhaps E–MAA ionomers undergo more than one process, including possibly water absorption, upon annealing at room temperature. Unfortunately, EXAFS may be of little use in distinguishing between these possibilities because of the carboxylate oxygen atoms, which might not be distinguishable from oxygen atoms of water by EXAFS.

## Conclusions

EXAFS studies of a novel cationomer during heating have shown that a DSC endotherm centered near 60 °C corresponded to a change in the second shell of the local environment surrounding the neutralizing anion while the first shell was unaffected. Although the details of the local environment are still under investigation, EXAFS results indicate that water was leaving the second coordination shell of the anion. By drying the sample under vacuum below the transition temperature, a small but measureable weight loss was found. Drying the sample in this manner also eliminated the DSC endotherm. These results suggest that the endothermic peak contains contributions from the energy change associated with water vaporization along with the energy change associated with water leaving the immediate coordination environment of the bromine. Arguments are also presented that the "ionic crystallite transition" found in ethylene–methacrylic acid copolymer ionomers might actually be the result of water absorption.

This study also emphasizes the extreme hydrophilicity of ionomers since the observed water absorption occurred in samples stored over dry $CaSO_4$. Such water sensitivity has also been noticed in EXAFS studies of carboxy-telechelic polyisoprenes[42] and sulfonated polyurethane ionomers.[43] Severe procedures may be necessary to prevent water absorption by ionomers such as those described by Painter and Coleman.[23]

**Acknowledgment.** This study would not have been possible without the extremely helpful people at SSRL and CHESS who answered our seemingly incessant questions. We would like to thank Richard S. Reiner for performing DSC experiments while the first two authors were at SSRL. Also, thanks to Mr. Matt Newville at the University of Washington for his help concerning FEFF5.

Financial support for this work comes from the Department of Energy under Grant DE-FG02-88ER45370. Finally, R.J.G. and B.P.G. would like to thank the Department of Defense for their fellowship support through the National Defense Science and Engineering Graduate Fellowship program.

## References and Notes

(1) Tant, M. R.; Wilkes, G. L. *J. Macromol. Sci., Rev. Macromol. Chem. Phys.* **1988**, *C28* (1), 1.
(2) Fitzgerald, J. J.; Weiss, R. A. *J. Macromol. Sci., Rev. Macromol. Chem. Phys.* **1988**, *C28* (1), 99.
(3) Lantman, C. W.; MacKnight, W. J.; Lundberg, R. D. *Annu. Rev. Mater. Sci.* **1989**, *19*, 295.
(4) Eisenberg, A.; King, M. *Ion-Containing Polymers*; Halsted-Wiley: New York, 1975.
(5) *Ionomers: Synthesis, Structure, Properties and Applications*; Tant, M. R., Wilkes, G. L., Mauritz, K. A., Eds. (to appear).
(6) Longworth, R.; Vaughn, D. J. *Polym. Prepr. (Am. Chem. Soc., Div. Polym. Chem.)* **1968**, *9*, 525.
(7) Marx, C. L.; Cooper, S. L. *J. Macromol. Sci., Phys.* **1974**, *B9* (1), 19.
(8) Holden, H. W. *J. Polym. Sci., Part C* **1964**, *6*, 53.
(9) Tadano, K.; Hirasawa, E.; Yamamoto, H.; Yano, S. *Macromolecules* **1989**, *22*, 226.
(10) Tadano, K.; Hirasawa, E.; Yamamoto, H.; Yano, S. *Macromolecules* **1989**, *22*, 2776.
(11) Tsunashima, K.; Nishioju, H.; Hirasawa, E.; Yano, S. *Polymer* **1992**, *33*, 1809.
(12) Pan, H. K.; Knapp, G. S.; Cooper, S. L. *Colloid Polym. Sci.* **1984**, *262*, 734.
(13) Tsunashima, K.; Kutsumizu, S.; Hirasawa, E.; Yano, S. *Macromolecules* **1991**, *24*, 5910.
(14) Kutsumizu, S.; Hashimoto, Y.; Yano, S.; Hirasawa, E. *Macromolecules* **1991**, *24*, 2629.
(15) Yano, S.; Nagao, N.; Hattori, M.; Hirasawa, E.; Tadano, K. *Macromolecules* **1992**, *25*, 368.
(16) Tachino, H.; Hara, H.; Hirasawa, E.; Kutsumizu, S.; Tadano, K.; Yano, S.; *Macromolecules* **1993**, *26*, 752.
(17) Hirasawa, E.; Yamamoto, Y.; Tadano, K.; Yano, S. *J. Appl. Polym. Sci.* **1991**, *42*, 351.
(18) Hirasawa, E.; Tadano, K.; Yano, S. *J. Polym. Sci., Part B: Polym. Phys.* **1991**, *29*, 753.
(19) Hirasawa, E.; Hamazaki, H.; Tadano, K.; Yano, S. *J. Appl. Polymn. Sci.* **1991**, *42*, 621.
(20) Painter, P. C.; Brozoski, B. A.; Coleman, M. M. *J. Polym. Sci., Polym. Phys. Ed.* **1982**, *20*, 1069.
(21) Brozoski, B. A.; Coleman, M. M.; Painter, P. C. *J. Polym. Sci., Polym. Phys. Ed.* **1983**, *21*, 301.
(22) Brozoski, B. A.; Coleman, M. M.; Painter, P. C. *Macromolecules* **1984**, *17*, 230.
(23) Brozoski, B. A.; Painter, P. C.; Coleman, M. M. *Macromolecules* **1984**, *17*, 1591.
(24) Kutsumizu, S.; Nagao, N.; Tadano, K.; Tachnio, H.; Hirasawa, E.; Yano, S. *Macromolecules* **1992**, *25*, 6829.
(25) Varma, S. C.; Ahsan, M. A.; George, M. H.; Barria, J. A. *Polym. Commun.* **1990**, *31*, 11.
(26) Goddard, R. J.; Grady, B. P.; Cooper, S. L. *Am. Chem. Soc., Polym. Mater. Sci. Eng.* **1993**, *68*, 308.
(27) Goddard, R. J.; Cooper, S. L. *J. Polym. Sci., Part B: Polym. Phys.*, in press.
(28) See for example: Stern, E. A *Phys. Rev. B* **1974**, *10*, 3027. Stern, E. A.; Sayers, D. E.; Lytle, F. W. *Phys. Rev. B* **1975**, *11*, 4836.
(29) Teo, B. K.; Lee, P. A. *J. Am. Chem. Soc.* **1979**, *101*, 2815.
(30) McKale, A. G.; Veal, B. W.; Paulikas, A. P.; Chan, S.-K.; Knapp, G. S. *Phys. Rev. B* **1988**, *38*, 10919.
(31) Teo, B. K. *EXAFS: Basic Principles and Data Analysis*; Springer-Verlag: New York, 1986; Chapter 5.
(32) For example, see ref 31, Chapter 6.
(33) Rehr, J. J.; Albers, R. C.; Zabinsky, S. I. *Phys. Rev. Lett.* **1992**, *69*, 3397.
(34) Stern, E. A.; Livins, P.; Zhang, Z. *Phys. Rev. B* **1991**, *43*, 8850.
(35) Grady, B. P.; Cooper, S. L. Submitted to *Macromolecules*.
(36) Powers, R.; Rudman, R. *J. Chem. Phys.* **1980**, *72*, 1630.
(37) Abrahams, S. C.; Bernstein, J. L. *Acta. Crystallogr.* **1977**, *B33*, 3601.
(38) Matt Newville, private communication.
(39) Yang, C. Z.; O'Connell, E. M.; Grady, B. P.; Cooper, S. L. *J. Polym. Sci., Polym. Phys. Ed.*, in press.
(40) Wyckoff, R. W. G. *Z. Kristallogr.* **1928**, *67*, 91.
(41) Kabisch, G. *J. Raman Spectrosco.* **1980**, *9*, 279.
(42) Register, R. A.; Foucart, M.; Jér°ome, R.; Ding, Y. S.; Cooper, S. L. *Macromolecules* **1988**, *21*, 1009.
(43) Ding, Y. S.; Register, R. A.; Yang, C. Z.; Cooper, S. L. *Polymer* **1989**, *30*, 1221.